
Article:
Wang, D., Zhang, S., Zhou, D. et al. (6 more authors) (2019) Temperature stable cold sintered (Bi0.95Li0.05)(V0.9Mo0.1)O4-Na2Mo2O7 microwave dielectric composites. Materials, 12 (9). 1370. ISSN 1996-1944

https://doi.org/10.3390/ma12091370

---

materials

MDPI

Article

Temperature Stable Cold Sintered $(Bi_{0.95}Li_{0.05})(V_{0.9}Mo_{0.1})O_4$-$Na_2Mo_2O_7$ Microwave Dielectric Composites

Dawei Wang [1,*], Shiyu Zhang [2], Di Zhou [3], Kaixin Song [1,4], Antonio Feteira [5], Yiannis Vardaxoglou [2], Will Whittow [2], Darren Cadman [2] and Ian M. Reaney [1,*]

[1] Department of Materials Science and Engineering, University of Sheffield, Sheffield S1 3JD, UK; kxsong@hdu.edu.cn (K.S.)
[2] Wolfson School of Mechanical, Electrical and Manufacturing Engineering, Loughborough University, Loughborough LE11 3TU, UK; S.Zhang@lboro.ac.uk (S.Z.); J.C.Vardaxoglou@lboro.ac.uk (Y.V.); W.G.Whittow@lboro.ac.uk (W.W.); D.A.Cadman@lboro.ac.uk (D.C.)
[3] Electronic Materials Research Laboratory, Key Laboratory of the Ministry of Education & International Center for Dielectric Research, Xi'an Jiaotong University, Xi'an 710049, Shaanxi, China; zhoudi1220@xjtu.edu.cn (D.Z.)
[4] College of Electronics Information, Hangzhou Dianzi University, Hangzhou 310018, China
[5] Christian Doppler Laboratory for Advanced Ferroic Oxides, Sheffield Hallam University, Sheffield S1 1WB, UK; a.feteira@shu.ac.uk (A.F.)
* Correspondence: dawei.wang@sheffield.ac.uk (D.W.); i.m.reaney@sheffield.ac.uk (I.M.R.)

Received: 6 March 2019; Accepted: 25 April 2019; Published: date

Abstract: Dense $(Bi_{0.95}Li_{0.05})(V_{0.9}Mo_{0.1})O_4$-$Na_2Mo_2O_7$ ((100−x) wt.% $(Bi_{0.95}Li_{0.05})(V_{0.9}Mo_{0.1})O_4$ (BLVMO)-x wt.% $Na_2Mo_2O_7$ (NMO) composite ceramics were successfully fabricated through cold sintering at 150 °C under at 200 MPa for 30 min. X-ray diffraction, back-scattered scanning electron microscopy, and Raman spectroscopy not only corroborated the coexistence of BLVMO and NMO phases in all samples, but also the absence of parasitic phases and interdiffusion. With increasing NMO concentration, the relative pemittivity (ε_r) and the Temperature Coefficient of resonant Frequency (TCF) decreased, whereas the Microwave Quality Factor (Qf) increased. Near-zero TCF was measured for BLVMO-20wt.%NMO composites which exhibited $\varepsilon_r \sim 40$ and $Qf \sim 4000$ GHz. Finally, a dielectric Graded Radial INdex (GRIN) lens was simulated using the range of ε_r in the BLVMO-NMO system, which predicted a 70% aperture efficiency at 26 GHz, ideal for 5G applications.

Keywords: cold sintering process; microwave dielectric ceramics; graded radial index lens

1. Introduction

Microwave (MW) dielectrics are used in wireless communication systems as resonators, filters, and capacitors [1]. For miniaturization and reliability, microwave devices are fabricated from Low/Ultra-Low Temperature Co-fired Ceramics (LTCC and ULTCC) due to their compatibility with sustainable and cheap electrodes such as Ag, Cu and Al [2–6]. Typically, MW ceramics have permittivity, $10 < \varepsilon_r < 100$, and quality factor, $2000 < Qf < 200{,}000$, depending on the precise application along with near-zero Temperature Coefficient of resonant Frequency (TCF < ±10 MK^{-1}) [7–12]. Dielectric resonators require ultra-high Qf (>40,000 GHz) and medium permittivity ($20 < \varepsilon_r < 50$) whereas LTCC typically have low ε_r (~10) and require only moderate Qf (~2000) for 3/4G mobile technology [7–12].

Recently, the Cold Sintering Process (CSP) has shown potential to densify ceramics/composites/devices at < 200 °C [13–23]. Kahari et al., densified Li_2MoO_4 (LMO) ceramics at room temperature by adding water and applying pressure to powders. CSP LMO ceramics exhibited

ε_r and *Qf* similar to conventional sintering [13]. Subsequently, CSP was studied by Guo et al. who applied this densification method to many different microwave materials and devices, including MoO_3, LMO, $Na_2Mo_2O_7$, $K_2Mo_2O_7$, $(LiBi)_{0.5}MoO_4$ and $Na_2Mo_2O_7$ (NMO)-xPTFE composites [17–24]. More recently, Hong et al. investigated the plastic deformation and densification of NaCl at room temperature [20], and Induja et al. densified Al_2SiO_5 ceramics using CSP with the addition of NaCl [21]. Our recent work has demonstrated that low TCF (−4.7 ppm/°C) and high *Qf* (16,000–22,000 GHz) could be achieved in $Na_{0.5}Bi_{0.5}MoO_4$-Li_2MoO_4 and magnetodielectric Li_2MoO_4-$BaFe_{12}O_{19}$ composites, respectively [22–24].

Among reported CSP microwave materials, only $Na_{0.5}Bi_{0.5}MoO_4$-Li_2MoO_4 composites have been shown to have near zero TCF but with a comparatively low ε_r (17.4) [22]. In the present work, $(Bi_{0.95}Li_{0.05})(V_{0.9}Mo_{0.1})O_4$ (BLVMO, ε_r = 76, TCF = +81 ppm/°C) and $Na_2Mo_2O_7$ (NMO, ε_r of 11.6, TCF of −99 ppm/°C) were selected as cold sintering end-members to fabricate a composite series with the anticipation for delivering a medium ε_r (*ca* 40-50), zero TCF ceramic suitable for MW applications [25–28]. The potential use CSP composites in a novel graded radial index (GRIN) dielectric lens is discussed.

2. Experimental Section

BLVMO and NMO powders were synthesized separately by solid-state reaction. Raw materials, including V_2O_5 (99+%, Acros Organics), MoO_3 (99+%, Acros Organics), Na_2CO_3 (99.9%, Fisher Scientific), Li_2CO_3 (99.9%, Sigma-Aldrich) and Bi_2O_3 (99.9%, Acros Organics)were batched and ball-milled in isopropanol for 4 h. Dried powders were calcined at 600 °C and 500 °C for BLVMO and NMO, respectively. To prepare (100−x) wt.% BLVMO-x wt.% NMO (x = 0, 5, 10, 20, 40, 50, 80, 100) composite ceramics, BLVMO and NMO powder was mixed with 5–10 wt.% deionized water. Mixtures were hot-pressed 30 min at 150 °C at 200 MPa and dried 24 h at 120 °C to remove residual moisture. In addition, BLVMO and NMO bulk ceramics were conventionally sintered at 690 and 610 °C, respectively.

Bulk densities of ceramic pellets were calculated by the geometric method. Crystal structure, phase assemblage, microstructures of ceramic pellets were characterised by X-ray powder diffraction (XRD, D2 Phaser, Bruker) using Cu$K\alpha$ radiation, scanning electron microscopy (SEM, Inspect F, FEI) and Raman spectroscopy (inVia Raman microscope, Renishaw) using a green laser with 514.5 nm at room temperature, respectively. Microwave properties of ceramic pellets were determined by a $TE_{01\delta}$ dielectric resonator method using a vector network analyzer (R3767CH, Advantest Corporation, Tokyo, Japan). A Peltier device heated the cavity to measure the resonant frequency (*f*) from 25 °C to 85 °C. TCF was calculated according to:

$$\mathrm{TCF} = \frac{f_T - f_{T_0}}{f_{T_0} \times (T - T_0)} \times 10^6 \quad (1)$$

where the f_T and f_{T_0} were the $TE_{01\delta}$ resonant frequencies at temperature T and T_0, respectively.

3. Results and Discussion

The bulk and relative densities of CSP BLVMO are 4.98 g/cm^3 and 73%, respectively, which increase to 6.04 g/cm^3 and 98% with the addition of NMO (Figure 1 and Table 1). Following an initial increase for x = 0.05, bulk densities decreased linearly due to a lower theoretical density of NMO compared with BLVMO (6.85 g/cm^3 and 3.69 g/cm^3 for BLVMO and NMO, respectively) [25–28]. The relative densities of (100−x) wt.% BLVMO-x wt.% NMO ceramics are >90% (except pure BLVMO), attaining 98% for 40 wt.% NMO, confirming that dense (100−x) wt.% BLVMO-x wt.% NMO composites could be readily fabricated by CSP.

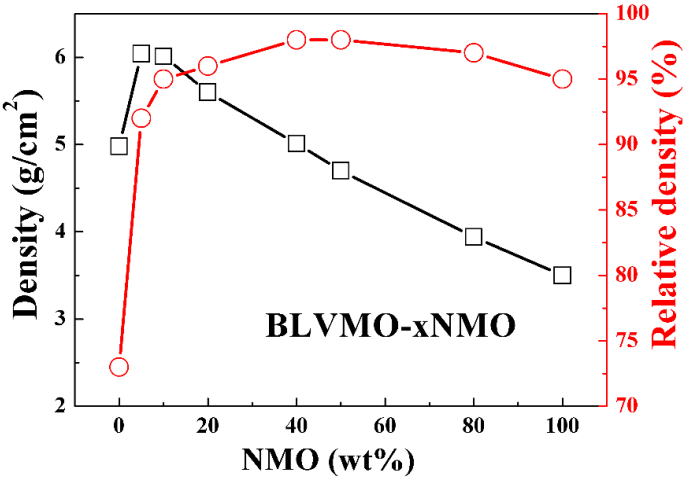

Figure 1. Bulk and relative densities of (100−x) wt.% $(Bi_{0.95}Li_{0.05})(V_{0.9}Mo_{0.1})O_4$ (BLVMO)-x wt.% $Na_2Mo_2O_7$ (NMO) ceramic composites.

Table 1. Sintering temperatures (ST), relative densities (ρ_r), and microwave dielectric properties of BLVMO, NMO and (100−x) wt.% BLVMO-x wt.% NMO ceramics.

Composition	ST (°C)	ρ_r (%)	ε_r	tanδ (%)	Qf (GHz)	TCF (ppm/°C)
BLVMO	150	73	30	0.003	1300	+61
5% NMO	150	92	48	0.0014	3565	+41
10% NMO	150	95	48	0.0012	3959	+20
20% NMO	150	96	40	0.0012	4000	+4
40% NMO	150	98	30	0.001	5000	−35
50% NMO	150	98	26	0.001	7000	−46
80% NMO	150	97	16	0.0007	10000	−76
NMO	150	95	12.7	0.0005	12000	−99
BLVMO	690	96	76	0.0006	7000	+81
NMO	610	87	11.6	0.0005	19000	−78

Room-temperature XRD patterns of CSP BLVMO, NMO and (100−x) wt.% BLVMO-x wt.% NMO samples in the 10°–50° 2θ range are shown in Figure 2. BLVMO has a tetragonal scheelite structure (PDF 48-0744) [26–28], with no evidence of splitting of main diffraction peaks. NMO has an orthorhombic structure with symmetry described by the space group *Cmca* (PDF 01-073-1797, a = 7.164 Å, b = 11.837 Å, c = 14.713 Å, Z = 8) [25]. All reflections in the XRD data for BLVMO-NMO ceramic composites can be ascribed to BLVMO and NMO and the intensity of NMO diffraction peaks increases with the concentration of NMO, as marked in Figure 2. Coexistence of peaks corresponding to BLVMO and NMO appear in all compositions with $0 < x < 1$, and there is no apparent shift in peak position, indicating no interaction between these two end-members.

Room-temperature Raman spectra of CSP BLVMO, NMO and (100−x) wt.% BLVMO-x wt.% NMO ceramics are shown in Figure 3. According to group theory and irreducible representations, there are 15 and 129 different vibrational modes in BLVMO and NMO [26–29], respectively, given as follows:

$$\Gamma_{BLVMO} = 3A_g + 2A_u + 6B_g + 4B_u \quad (2)$$

$$\Gamma_{NMO} = 18A_g + 13A_u + 15B_{1g} + 19B_{1u} + 14B_{2g} + 18B_{2u} + 19B_{3g} + 13B_{3u} \quad (3)$$

In BLVMO, nine $3A_g + 6B_g$ modes are Raman active and six $2A_u + 4B_u$ modes are IR active [26–28]. In NMO, translations of Na and Mo atoms give $3A_g + 2A_u + 3B_{1g} + 4B_{1u} + 3B_{2g} + 4B_{2u} + 3B_{3g} + 2B_{3u}$ and $3A_g + 2A_u + 3B_{1g} + 4B_{1u} + 2B_{2g} + 3B_{2u} + 4B_{3g} + 3B_{3u}$ modes, respectively. Three $B_{1u} + B_{2u} + B_{3u}$ modes are acoustic active and the remaining $12A_g + 9A_u + 9B_{1g} + 12B_{1u} + 9B_{2g} + 12B_{2u} + 19B_{3g} + 9B_{3u}$ modes correspond to stretching and bending modes of MoO_4 and MoO_6 octahedra [29]. The Raman spectra

of (100−x) wt.% BLVMO-x wt.% NMO composites consist of a superposition of the spectral features exhibited by each individual phase, further confirming the coexistence of BLVMO and NMO in composite ceramics. Furthermore, the intensity of the NMO Raman modes increases with increasing NMO concentration. Several Raman bands in NMO (~86, 832, 872, 920 and 937 cm^{-1}) are visible in all (100−x) wt.% BLVMO-x wt.% NMO compositions, confirming the coexistence of BLVMO and NMO in the composites.

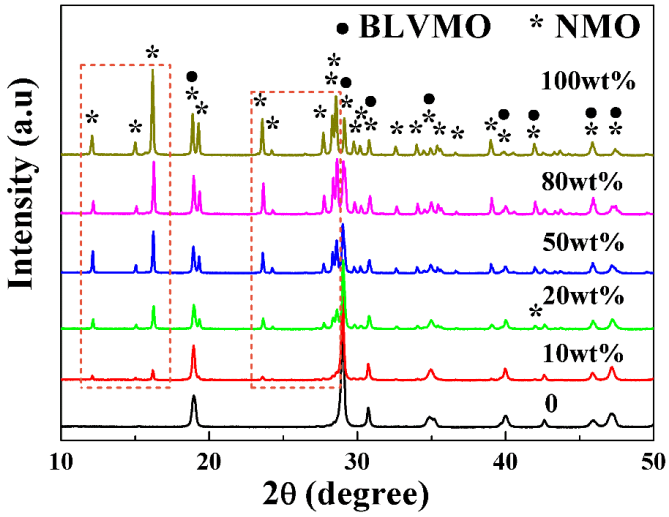

Figure 2. X-ray diffraction (XRD) patterns of (100−x) wt.% BLVMO-x wt.% NMO ceramic composites.

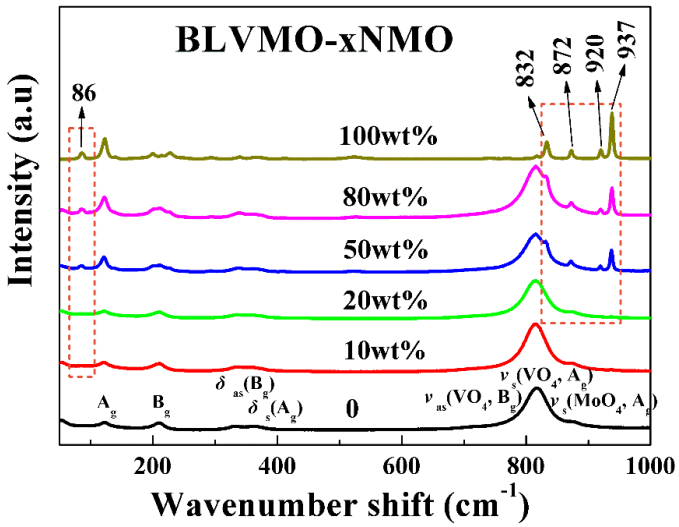

Figure 3. Raman spectra of (100−x) wt.% BLVMO-x wt.% NMO ceramic composites.

Back-Scattered Electron (BSE) scanning electron microscope images of fracture surfaces of conventionally-sintered BLVMO, cold-sintered BLVMO-20wt.%NMO and NMO are revealed in Figure 4. Dense microstructures are visible in all three compositions, in agreement with the data presented in Figure 1 and Table 1. The average grain size of BLVMO (1–2 μm, Figure 1a) is smaller than that of NMO (2–5 μm, Figure 1b), consistent with previous reports [25–28]. Figure 4c,d shows the composites to be composed two chemically distinct and discrete phases with EDS confirming the dark and light contrast to be NMO and BLVMO, respectively, in agreement with XRD and Raman (Figures 2 and 3).

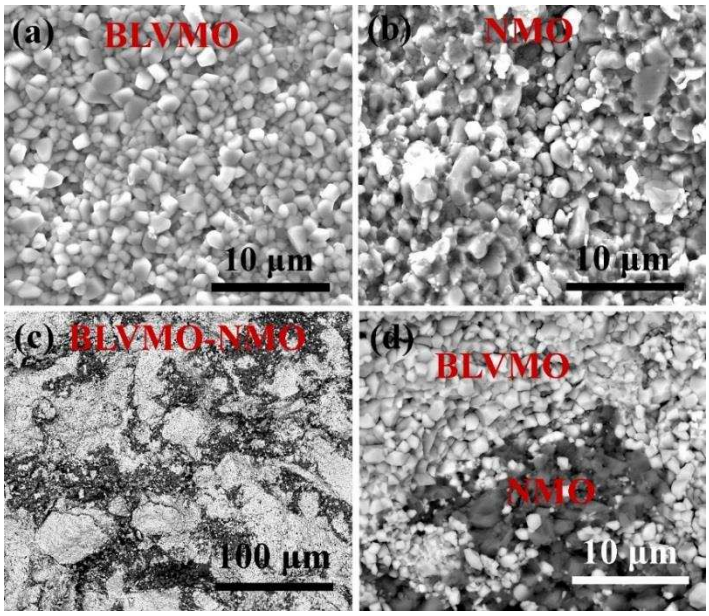

Figure 4. The SEM and BSE images of (**a**) conventionally-sintered BLVMO, (**b**) cold-sintered NMO, and (**c**,**d**) cold-sintered BLVMO-20 wt.%NMO samples.

The microwave properties of (100−x) wt.% BLVMO-x wt.% NMO as a function x are presented in Figure 5 and also listed in Table I. Low relative density (73%) of CSP BLVMO is observed which gives rise to lower ε_r (30) and *Qf* (1300 GHz) than for conventionally-sintered BLVMO, Table 1. ε_r and TCF values decrease linearly from 48 and +41 ppm/°C, respectively, for BLVMO-5 wt.%NMO to 12.7 and −99 ppm/°C for NMO. Near-zero TCF (−4 ppm/°C) is obtained for BLVMO-20 wt.%NMO. *Qf* increases from 1300 GHz for BLVMO to 12,000 GHz for NMO, as shown in Figure 5 and Table 1.

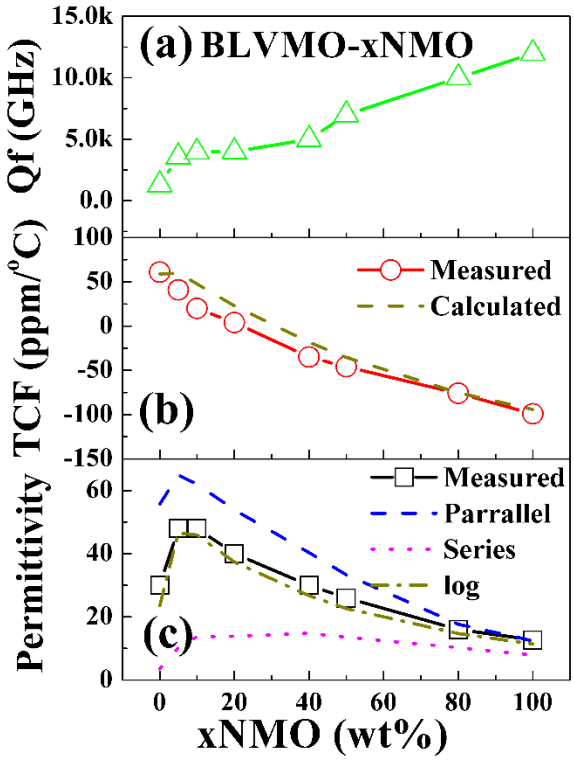

Figure 5. The microwave properties of (100−x) wt.% BLVMO-x wt.% NMO ceramic composites as a function of x (NMO fraction). (a) *Qf*, (b) TCF, (c) ε_r.

Provided there are no chemical reactions between phases, the ε_r in composites may be predicted by different mixing laws, as follows [22]:

$$\text{parallel mixing law, } \varepsilon = V_1\,\varepsilon_1 + V_2\,\varepsilon_2 + V_0\,\varepsilon_0 \quad (4)$$

$$\text{series mixing law, } 1/\varepsilon = V_1/\varepsilon_1 + V_2/\varepsilon_2 + V_0/\varepsilon_0 \quad (5)$$

$$\text{logarithmic mixing law, } \varepsilon = \varepsilon_1^{V_1}\varepsilon_2^{V_2}\varepsilon_0^{V_0} \text{ i.e., } \lg\varepsilon = V_1\lg\varepsilon_1 + V_2\lg\varepsilon_2 + V_0\lg\varepsilon_0 \quad (6)$$

where ε_1, ε_2 and ε_0 are the ε_r of phase 1, phase 2 and air, respectively and V_1, V_2 and V_0 ($V_1 + V_2 + V_0 = 1$) are their respective volume fractions. As shown in Figure 5, ε_r for (100−x) wt.% BLVMO-x wt.% NMO composite ceramics is within the range of calculated values for Equations (4) and (5), and close to the values obtained using Equation (6), indicating that ε_r follows a logarithmic mixing law with x. TCF of composites is predicted with a simple mixing rule, which is derived from the Equation (6) [30]:

$$\text{TCF} = V_1\text{TCF}_1 + V_2\text{TCF}_2 \quad (7)$$

where TCF_1 and TCF_2 correspond to the TCF of the two phases. TCF is consistent with calculated values using Equations (7), as shown in Figure 5b, suggesting they can be predicted using simple rules of mixture.

Microwave dielectric properties of various cold-sintered microwave dielectric materials are compared in Table 2. Numerous materials (ρ_r = 83.7%-100%) with a range of dielectric properties (2.1 ≤ ε_r ≤ 48, 2240 ≤ Qf ≤ 135,700 GHz, −174 ≤ TCF ≤ 184 ppm/°C) can be densified, indicating that CSP is an effective, and energy-saving strategy for the fabrication of microwave devices [31,32]. (100−x) wt.% BLVMO-x wt.% NMO (x = 10–20) exhibits the highest value of ε_r (~48) for near-zero TCFs cold-sintered microwave dielectric materials and is thus attractive for RF applications.

Table 2. Comparison of relative densities, and microwave properties of cold-sintered microwave dielectric materials (* unpublished work, ρ_r = relative density, PTFE = Polytetrafluoroethylene, LMO = Li_2MoO_4, BF12 = $BaFe_{12}O_{19}$, NBMO = $Na_{0.5}Bi_{0.5}MoO_4$, BLVMO = $(Bi_{0.95}Li_{0.05})(V_{0.9}Mo_{0.1})O_4$, NMO = $Na_2Mo_2O_7$).

Compound	ρ_r (%)	ε_r	$Q \times f$ (GHz)	TCF (ppm/°C)	reference
PTFE	100	2.12	135,700	+60	*
Polystyrene	100	2.53	24,320	−5	*
Al_2SiO_5-NaCl	/	4.52	22,350	−24	[21]
KCl	98	4.74	7738	−149	*
LMO	95.5	5.1–5.61	10,200-30,500	−170	[13–19,22]
NaCl	97–99	5.22–5.55	12,000-49,600	−100	[20,21]
LMO-15%BF12	94.1	5.8	17,430	-	[23]
K_2MoO_4	100	6.37	26,500	−70	*
$AgNaMoO_4$	90.8	9.3	7078	−120	*
$K_2Mo_2O_7$	94.1–96	9.35–9.8	12,000–16,000	−63	[17,*]
MoO_3	83.7	9.91	11,800	−39	[24]
$Na_2Mo_2O_7$	93.7–95	12.7–13.4	12,000–14,900	−99	[17], *
NBMO-20%LMO	93.6	17.4	7470	−4.7	[22]
NBMO-10%LMO	92.6	24.1	2240	+15	[22]
$(LiBi)_{0.5}MoO_4$	88	33.7–37	1700–2300	+180	[18]
BLVMO-20%NMO	96	40	4000	+4	this work
BLVMO-10%NMO	95	48	3959	+20	this work

The low sintering temperature and absence of lateral shrinkage suggest that (100−x) wt.% BLVMO-x wt.% NMO composites have the potential for many novel RF applications including antennas, temperature stable capacitors, LTCC substrates and GRaded INdex (GRIN) dielectric lenses.

A GRIN lens is an antenna component for transforming a spherical to a planar wavefront, and enables highly directive antennas and shaped beams. A lightweight, flat lens may be used in the proximity of the feed to realise a compact system that is desired by 5G applications. For practical fabrication, the index profile of a flat lens is usually graded to several tight-fitted rings with radially reduced ε_r. GRIN lenses may be fabricated from concentric dielectric cylindrical rings with graded ε_r, Figure 6a. The simulated electric field of a ceramic GRIN lens is displayed in Figure 6b, transforming a spherical to a planar wavefront at 26 GHz.

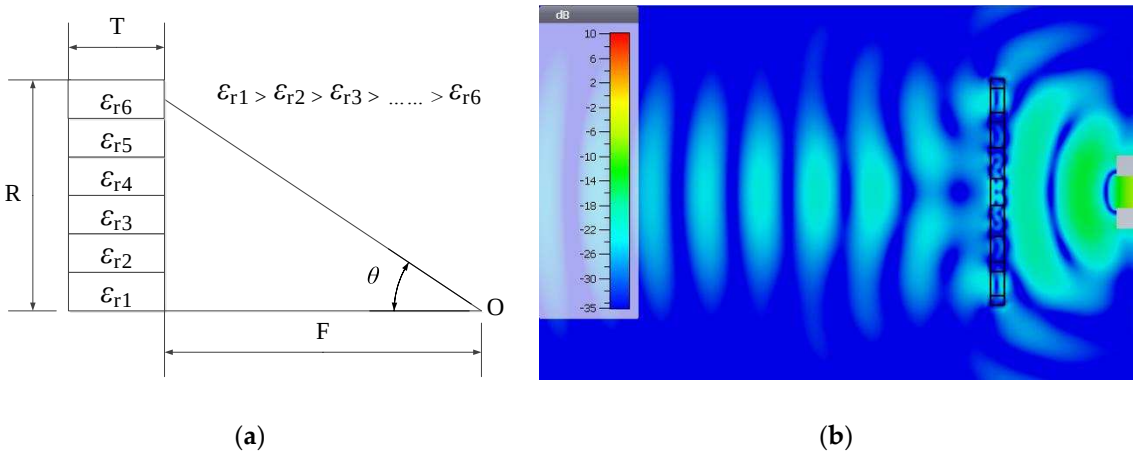

(**a**) (**b**)

Figure 6. (**a**) Lens design principle; (**b**) Simulated electric field of a ceramic Graded Radial INdex (GRIN) lens that transforming spherical wavefronts into a planar wavefront at 26 GHz.

The design parameters of a lens are shown in Tables 3 and 4. The dielectric lens is comprised of six concentric rings; the outermost has the lowest effective ε_r (12.7), while the centre has the highest ε_r (48). The high ε_r ceramic reduces the thickness of the lens (miniaturises) compared with low ε_r materials such as polymers.

Table 3. Designed parameters of a 3D-printed lens.

Parameter	Value
Diameter	R = 12.5 mm
Focal length	F = 12.5 mm
Thickness	T = 1.53 mm

Table 4. Dielectric constant values of the concentric dielectric rings.

Ring No.	ε_r	Ring Outer Radius(mm)
1	48	1.1
2	40	4.9
3	30	7.8
4	26	8.8
5	16	11.5
6	12.7	12.5

Lens performance was simulated using CST Microwave Studio. An open-ended *Ka*-band waveguide (7.112 mm × 3.556 mm) was used to illuminate the lens. The boresight directivity is increased across the whole frequency range from 26 to 40 GHz. The relative increase compared to the case with no lens is between 4.6 and 8.5 dB . The aperture efficiency of the lens is ~70% at 26 GHz.

The simulated E-plane (i.e., the plane containing the electric field vector) and H-plane (the plane containing the magnetic field vector, normal to the E-plane) radiation patterns of the lens are illustrated in Figure 7.

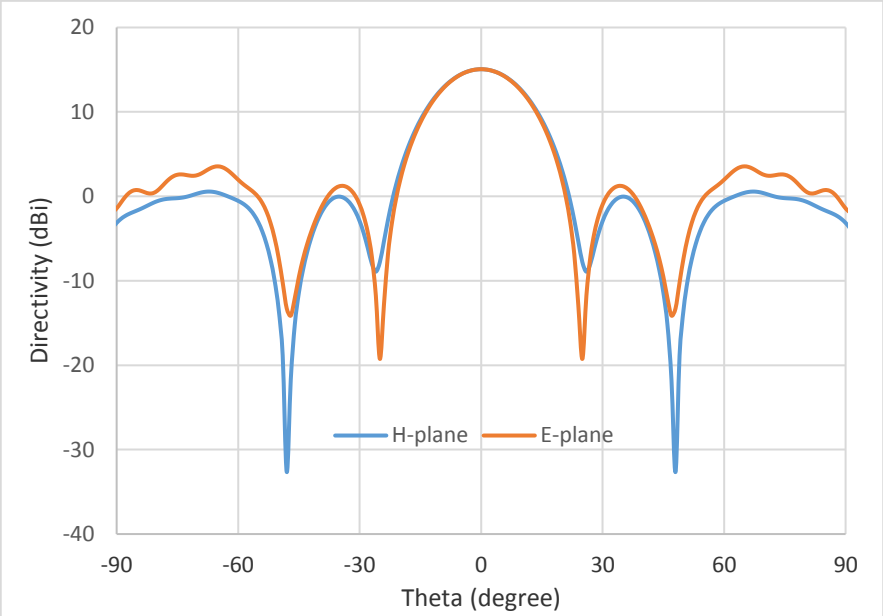

Figure 7. Simulated far-field radiation patterns of the ceramic GRIN lens at 26 GHz.

4. Conclusions

The (100−x) wt.% BLVMO-x wt.% NMO ceramics with relative density of 92%–98% were fabricated by cold sintering process at 150 °C/30 min/200 MPa. No evidence of chemical interaction was observed in composites, except BLVMO and NMO phases, by means of SEM, XRD and Raman spectroscopy. As x increased, TCF and ε_r decreased, while *Qf* increased. Near-zero TCF ~ +4 ppm/°C was measured for BLVMO-20wt%NMO with ε_r ~ 40 and *Qf* ~ 4000 GHz. A dielectric GRIN lens was designed and simulated exhibiting 70% aperture efficiency at 26 GHz, which we propose may be fabricated using (100−x) wt.% BLVMO-x wt.% NMO composites.

Author Contributions: Experiments and writing-original draft preparation, D. W.; Lens design and simulation, S. Z., Y. V., D. C. and W. W.; Supervision, I. M. R.; Data discussion, D. Z., K. S. and A. F.; Writing-review and editing, I.M.R and A. F.

Funding: We acknowledge the EPSRC grants, EP/N010493/1 and EP/L017563/1, "Synthesizing 3D Metamaterials for RF, Microwave and THz Applications" and "Sustainability and Substitution of Functional Materials and Devices" supporting this work.

Conflicts of Interest: The authors declare no conflict of interest.

References

1. Reaney, I.M.; Iddles D. Microwave dielectric ceramics for resonators and filters in mobile phone networks. *J. Am. Ceram. Soc.* **2006**, *89*, 2063–2072.
2. Sebastian, M.T.; Wang H.; Jantunen H. Low temperature co-fired ceramics with ultra-low sintering temperature: A review. *Curr. Opi. Solid State Mater. Sci.* **2016**, *20*, 151–170.
3. Zhou, D.; Pang, L.; Wang, D; Reaney, I.M. $BiVO_4$ based high k microwave dielectric materials: a review. *J. Mater. Chem. C* **2018**, *6*, 9290–9313.
4. Zhou, D.; Pang, L.; Wang, D; Qi, Z.; Reaney, I.M. High quality factor, ultralow sintering temperature $Li_6B_4O_9$ microwave dielectric ceramics with ultralow density for antenna substrates, *ACS Sustainable Chem. Eng.* **2018**, *6*, 11138–11143.

5. Pang, L.; Zhou, D.; Wang, D.; Zhao, J.; Liu, W.; Yue, Z.; Reaney, I.M. Temperature stable $K_{0.5}(Nd_{1-x}Bi_x)_{0.5}MoO_4$ microwave dielectrics ceramics with ultra-low sintering temperature. *J. Am. Ceram. Soc.* **2018**, *101*, 1806–1810.
6. Zhou, D.; Pang, L.; Wang, D.; Guo, H.; Yang, F.; Qi, Z.; Li, C.; Jin, B.; Reaney, I.M. Crystal structure, impedance and broadband dielectric spectra of ordered scheelite-structured $Bi(Sc_{1/3}Mo_{2/3})O_4$ ceramic. *J. Euro. Ceram. Soc.* **2018**, *38*, 1556–1561.
7. Pang, L.X.; Zhou, D.; Qi, Z.M.; Liu, W.G.; Yue Z. X.; Reaney, I.M. Structure–property relationships of low sintering temperature scheelite-structured $(1-x)BiVO_4–xLaNbO_4$ microwave dielectric ceramics. *J. Mater. Chem. C* **2017**, *5*, 2695–2701.
8. Zhou, D.; Guo, D.; Li, W.B.; Pang, L.X.; Yao, X.; Wang D. W.; Reaney, I.M. Novel temperature stable high-ε_r microwave dielectrics in the $Bi_2O_3–TiO_2–V_2O_5$ system. *J. Mater. Chem. C* **2016**, *4*, 5357–5362.
9. Zhou, D.; Li, W.B.; Xi, H.H.; Pang L. X.; Pang G. S. Phase composition, crystal structure, infrared reflectivity and microwave dielectric properties of temperature stable composite ceramics (scheelite and zircon-type) in $BiVO_4$-YVO_4 system. *J. Mater. Chem. C* **2015**, *3*, 2582–2588.
10. Zhou, D.; Li, J.; Pang, L.X.; Chen, G.H.; Qi, Z.M.; Wang D. W.; Reaney, I.M. Crystal structure, infrared spectra, and microwave dielectric properties of temperature-stable Zircon-yype $(Y,Bi)VO_4$ solid solution ceramics. *ACS Omega* **2016**, *1*, 963–970.
11. Ma, J.L.; Fu, Z.F.; Liu, P.; Zhao, L.P.; Guo, B.C. Ultralow-fired $Li_2Mg_3TiO_6$-$Ca_{0.8}Sr_{0.2}TiO_3$ composite ceramics with temperature stable at microwave frequency. *J. Alloys Comp*. **2017**, *709*, 299–303.
12. Chen, G.H.; Gu, F.F.; Pan, M.; Yao, L.Q.; Li, M.; Chen, X.; Yang, Y.; Yang, T.; Yuan C. L.; Zhou, C.R. Microwave dielectric properties of $BiVO_4/Li_{0.5}Re_{0.5}WO_4$ (Re = La, Nd) ultra-low firing ceramics. *J. Mater. Sci.: Mater. Electron.* **2015**, *26*, 6511–6517.
13. Kahari, H.; Teirikangas, M.; Juuti J.; Jantunen, H. Dielectric properties of lithium molybdate ceramic fabricated at room temperature. *J. Am. Ceram. Soc.* **2014**, *97*, 3378–3379.
14. Kähäri, H.; Teirikangas, M.; Juuti, J.; Jantunen, H. Room-temperature fabrication of microwave dielectric $Li_2MoO_4–TiO_2$ composite ceramics. *Ceram. Inter.* **2016**, *42*, 11442–11446.
15. Väätäjä, M.; Kähäri, H,; Juuti, J.; Jantunen, H. Li_2MoO_4-based composite ceramics fabricated from temperature- and atmosphere-sensitive MnZn ferrite at room temperature. *J. Am. Ceram. Soc.* **2017**, *100*, 3626–3635.
16. Väätäjä, M.; Kähäri, H.; Ohenoja, K.; Sobocinski, M.; Juuti, J.; Jantunen, H. 3D printed dielectric ceramic without a sintering stage. *Sci. Rep.* **2018**, *8*, 15955.
17. Guo, J.; Guo, H.; Baker, A.L.; Lanagan, M.T.; Kupp, E.R.; Messing G. L.; Randall, C.A. Cold sintering: a paradigm shift for processing and integration of ceramics. *Angew. Chem. Int. Ed.* **2016**, *55*, 11457–11461.
18. Guo, J.; Baker, A.L.; Guo, H.; Lanagan M. T.; Randall, C.A. Cold sintering process: A new era for ceramic packaging and microwave device development. *J. Am. Ceram. Soc.* **2017**, *100*, 669–677.
19. Guo, J.; Berbano, S.S.; Guo, H.; Baker, A.L.; Lanagan M. T.; Randall, C.A. Cold sintering process of composites: bridging the processing temperature gap of ceramic and polymer materials. *Adv. Funct. Mater.* **2016**, *26*, 7115–7121.
20. Hong, W.; Li, L.; Cao, M.; Chen, X.M. Plastic deformation and effects of water in room-temperature cold sintering of NaCl microwave dielectric ceramics. *J. Am. Ceram. Soc.* **2018**, *101*, 4038–4043.
21. Induja I. J.; Sebastian, M.T. Microwave dielectric properties of mineral sillimanite obtained by conventional and cold sintering process. *J. Euro. Ceram. Soc.* **2017**, *37*, 2143–2147.
22. Wang, D.; Zhou, D.; Zhang, S.; Vardaxoglou, Y.; Whittow, W.G.; Cadman, D.; Reaney, I.M. Cold-sintered temperature stable $Na_{0.5}Bi_{0.5}MoO_4–Li_2MoO_4$ microwave composite ceramics. *ACS Sustainable Chem. Eng.* **2018**, *6*, 2438–2444.
23. Faouri, S.S.; Mostaed, A.; Dean, J.S.; Wang, D.; Sinclair, D.C.; Zhang, S.; Whittow, W.G.; Vardaxoglou, Y.; Reaney, I.M. High quality factor cold sintered $Li_2MoO_4–BaFe_{12}O_{19}$ composites for microwave applications. *Acta Mater.* **2019**, *166*, 202–207.
24. Zhou, D.; Pang, L.; Wang, D.; Reaney, I.M. Novel water-assisting low firing MoO_3 microwave dielectric ceramics. *J. Euro. Ceram. Soc.* **2019**, *39*, 2374–2378.
25. Zhang, G.Q.; Wang, H.; Guo, J.; He, L.; Wei, D.D.; Yuan, Q.B. Ultra-low sintering temperature microwave dielectric ceramics based on Na_2O-MoO_3 binary system. *J. Am. Ceram. Soc.* **2015**, *98*, 528–533.
26. Zhou, D.; Qu, W.G.; Randall, C.A.; Pang, L.X.; Wang, H.; Wu, X.G.; Guo, J.; Zhang, G.Q.; Shui, L.; Wang, Q.P.; Liu, H.C.; Yao, X. Ferroelastic phase transition compositional dependence for solid-solution

[$(Li_{0.5}Bi_{0.5})_xBi_{1-x}$][$Mo_xV_{1-x}$]$O_4$ scheelite-structured microwave dielectric ceramics. *Acta Mater.* **2011**, *59*, 1502–1509.

27. Zhou, D.; Pang, L.X.; Qu, W.G.; Randall, C.A.; Guo, J.; Qi, Z.M.; Shao, T.; Yao, X. Dielectric behavior, band gap, in situ X-ray diffraction, Raman and infrared study on (1−x)$BiVO_{4-x}$($Li_{0.5}Bi_{0.5}$)MoO_4 solid solution. *RSC Adv.* **2013**, *3*, 5009–5014.
28. Zhou, D.; Randall, C.A.; Wang, H.; Pang, L.X.; Yao, X. Ultra-low firing high-k scheelite structures based on [$(Li_{0.5}Bi_{0.5})_xBi_{1-x}$][$Mo_xV_{1-x}$]O4 microwave dielectric ceramics. *J. Am. Ceram. Soc.* **2010**, *93*, 2147–2150.
29. Saraiva, G.D.; Paraguassu, W.; Maczka, M.; Freire, P.T.C.; de Sousad, F.F.; Mendes Filho, J. Temperature-dependent Raman scattering studies on Na2Mo2O7 disodium dimolybdate. *J. Raman Spectrosc.* **2011**, *42*, 1114–1119.
30. Pang, L.X.; Wang, H.; Zhou, D.; Yao, X. A new temperature stable microwave dielectric with low-firing temperature in Bi_2MoO_6–TiO_2 system. *J. Alloys Comp*. **2010**, *493*, 626–629.
31. Wang, D.; Zhou, D.; Song, K.; Feteira, A.; Randall, C.A.; Reaney, I.M. Cold Sintered C0G Multilayer Ceramic Capacitors. *Adv. Electro. Mater. 2019. DOI: 10.1002/aelm.201900025*.
32. Ibn-Mohammed, T.; Randall, C.A.; Mustapha, K.B.; Guo, J.; Walker, J.; Berbano, S.; Koh, S.C.L.; Sinclair, D.C.; Reaney, I.M. Decarbonising ceramic manufacturing: a techno-economic analysis of energy efficient sintering technologies in the functional materials sector. *J. Euro. Ceram. Soc.* **Year** (if available), submitted.